European Journal of Cell Biology 102 (2023) 151314

Contents lists available at ScienceDirect

European Journal of Cell Biology

journal homepage: www.elsevier.com/locate/ejcb

Detection of Ras nanoclustering-dependent homo-FRET using fluorescence anisotropy measurements

Ganesh babu Manoharan [a], Camilo Guzmán [b], Arafath Kaja Najumudeen [c], Daniel Abankwa [a,*]

[a] Cancer Cell Biology and Drug Discovery group, Department of Life Sciences and Medicine, University of Luxembourg, Esch-sur-Alzette, Luxembourg
[b] Euro-BioImaging ERIC, Statutory Seat, Turku, Finland
[c] Institute of Biotechnology, HiLIFE Helsinki Institute of Life Science, University of Helsinki, Helsinki, Finland

ARTICLE INFO

Keywords:
Ras
Nanoclustering
Homo-FRET
Anisotropy
Drug discovery

ABSTRACT

The small GTPase Ras is frequently mutated in cancer and a driver of tumorigenesis. The recent years have shown great progress in drug-targeting Ras and understanding how it operates on the plasma membrane. We now know that Ras is non-randomly organized into proteo-lipid complexes on the membrane, called nanoclusters. Nanoclusters contain only a few Ras proteins and are necessary for the recruitment of downstream effectors, such as Raf. If tagged with fluorescent proteins, the dense packing of Ras in nanoclusters can be analyzed by Förster/fluorescence resonance energy transfer (FRET). Loss of FRET can therefore report on decreased nanoclustering and any process upstream of it, such as Ras lipid modifications and correct trafficking. Thus, cellular FRET screens employing Ras-derived fluorescence biosensors are potentially powerful tools to discover chemical or genetic modulators of functional Ras membrane organization. Here we implement fluorescence anisotropy-based homo-FRET measurements of Ras-derived constructs labelled with only one fluorescent protein on a confocal microscope and a fluorescence plate reader. We show that homo-FRET of both H-Ras- and K-Ras-derived constructs can sensitively report on Ras-lipidation and -trafficking inhibitors, as well as on genetic perturbations of proteins regulating membrane anchorage. By exploiting the switch I/II-binding Ras-dimerizing compound BI-2852, this assay is also suitable to report on the engagement of the K-Ras switch II pocket by small molecules such as AMG 510. Given that homo-FRET only requires one fluorescent protein tagged Ras construct, this approach has significant advantages to create Ras-nanoclustering FRET-biosensor reporter cell lines, as compared to the more common hetero-FRET approaches.

1. Introduction

The Ras-MAPK pathway is aberrantly upregulated in cancer and developmental diseases called RASopathies (Castel et al., 2020). Recent progress in the development of direct Ras inhibitors has added a long sought-after weapon against mutant Ras (Punekar et al., 2022). Covalent inhibitors against the KRAS-G12C mutation, such as approved sotorasib (AMG 510), realize the ideal approach of drug targeting only the mutant oncogene, while sparing its wild-type counterpart. These novel therapeutics allowed to test the prevailing cancer treatment and drug development concept, which is to pharmacologically correct the aberrant activity of the driving mutation. While indeed initially impressive responses in KRAS-G12C mutant lung cancer patients were observed with sotorasib, resistances inevitably emerge as with other targeted therapies (Punekar et al., 2022). This sobering realization necessitates continuing research efforts to understand and target the Ras pathway even more fundamentally.

Ras proteins are small GTPases, which switch conformation upon GTP-binding, allowing them to bind to recognition domains of effectors, such as the Ras binding domain (RBD) of the effector Raf (Simanshu et al., 2017). For proper effector activation, additional effector domains typically have to engage with the plasma membrane, where Ras is localized. In line with this membrane recruitment requirement, it was realized very early that inhibition of Ras plasma membrane localization shuts down Ras activity (Cox et al., 2015). Therefore, the first clinically tested Ras inhibitor developments aimed at the inhibition of Ras membrane anchorage.

Ras trafficking to the plasma membrane requires multiple steps of C-terminal post-translational modifications, which lead to a farnesylated and carboxymethylated terminal cysteine (Pavic et al., 2022). These

* Corresponding author.
E-mail address: daniel.abankwa@uni.lu (D. Abankwa).

https://doi.org/10.1016/j.ejcb.2023.151314
Received 13 December 2022; Received in revised form 10 March 2023; Accepted 10 April 2023
Available online 11 April 2023

modifications are recognized by trafficking chaperones of Ras, such as PDE6D (also known as PDE δ) and calmodulin (Chandra et al., 2011; Grant et al., 2020). These chaperones solubilize Ras in the cytoplasm thus facilitating its diffusion across the cell, eventually allowing for trapping on the Golgi or the recycling endosome and vesicular transport of Ras to the plasma membrane (Schmick et al., 2015).

The approximately 20 residue long C-terminus of Ras is highly divergent between isoforms and correspondingly named hypervariable region (hvr). Hence, differences in the biology of Ras isoforms must to a large extent somehow be encoded in this hvr. In conjunction with the second most divergent region, the helix α 4, the hvr also guides conformational changes of Ras on the membrane (Abankwa et al., 2010; Abankwa et al., 2008; Gorfe et al., 2007). These changes can affect signaling and membrane organization of Ras (Guzman et al., 2014b; Solman et al., 2015).

An exquisite plasma membrane lipid selectivity of the K-Ras4B (hereafter K-Ras) hvr was recently elucidated by the Hancock group, showing that several conformational states allow specific lysines of the K-Ras C-terminus to bind to specific phospholipid species of the membrane (Zhou et al., 2017). They furthermore demonstrated that in particular the co-clustering of K-Ras with asymmetric phosphatidylserine species is highly relevant for K-Ras function and membrane organization into nanocluster (Zhou et al., 2021). Global modulation of these lipid species can represent a novel approach to tackle *KRAS* mutant cancers (Kattan et al., 2021).

Ras nanocluster were first defined as isoform-specific, laterally segregated, non-random and transient (lifetimes up to 1 s) assemblies of about half-a-dozen Ras proteins that are recruitment sites for Ras effectors, thus affording distinct signaling output properties to the system (Abankwa and Gorfe, 2020). Interestingly, even the lipid-modified hvr alone displays a non-random, clustered distribution in silico and in cells (Li et al., 2012; Prior et al., 2003). Evidence for such lipid-anchor driven nanoclusters has also been gathered for other peripheral membrane proteins, such as Rho, Rab, Src-family and heterotrimeric G-proteins (Abankwa and Vogel, 2007; Kohnke et al., 2012; Najumudeen et al., 2013).

When Ras is activated, its mobility on the plasma membrane changes dramatically. Single molecule studies have revealed that its diffusion in the membrane slows and that the effector Raf is recruited to relatively immobile Ras (Murakoshi et al., 2004). Given that Raf co-clusters in Ras nanocluster and the fraction of Ras in nanoclusters correlates with the slow/ immobile fraction of Ras, it is plausible to assume that immobile Raf-associated active signaling nanoclusters exist (Abankwa and Gorfe, 2020). Properties of these active nanoclusters can be modulated by nanocluster scaffolds, such as galectin-1 and galectin-3 (Pavic et al., 2022), which are the best studied proteins of this type. We previously showed that galectin-1 binds to the RBD of effectors and provided evidence that it can somehow increase the active fraction of Raf that is engaged within Ras nanocluster (Blazevits et al., 2016). Supported by single molecule studies (Nan et al., 2015), a model could be derived which predicts Raf-dimers coupled to transient Ras-dimers as minimal units of active nanoclusters and MAPK-signaling (Blazevits et al., 2016). Of note, affinities between various proposed dimer interfaces of Ras have proven too weak for stable dimers to exist in solution, hence only transient, nanoclustering associated Ras dimers are plausible (Abankwa and Gorfe, 2020). Classically nanoclusters were identified using image analysis of electron micrographs of fixed plasma membrane sheets that were ripped-off from cells (Prior et al., 2003). These data were significantly supported by fluorescence microscopy methods, in particular Förster/ fluorescence resonance energy transfer (FRET) studies (Guzman et al., 2014a; Posada et al., 2016; Sarkar-Banerjee et al., 2017).

FRET is the non-radiative energy transfer between two fluorophores with suitable spectroscopic parameters and orientations, that occurs if their distance is below approximately 10 nm (Parkkola et al., 2021). Typically, two different fluorophores, the donor and acceptor, are genetically fused to Ras or its membrane anchoring hvr. The energy donor usually has an emission spectrum further in the blue, such as mGFP (the monomeric variant of EGFP), while the energy acceptor has an overlapping excitation spectrum further in the red, such as for instance mCherry. The energy transfer that can occur between non-like fluorophores is called hetero-FRET and can be detected by changes in the intensities and fluorescence lifetimes of the associated fluorophores (Guzman et al., 2016; Parkkola et al., 2021). Another way of measuring hetero-FRET is fluorescence-polarization or -anisotropy (Rizzo and Piston, 2005). Given the large size, the emission of fluorescence proteins is highly polarized (Rizzo et al., 2004). If two FRET-fluorophores are in FRET-proximity, initially polarized light becomes more depolarized after resonance energy transfer as the orientation of the acceptor fluorophore is likely to be different from that of the donor. The fluorescence polarization signal or anisotropy signal, which is another measure and expression for polarization, requires measurements on instruments that can generate and detect light with two different polarizations.

FRET can also occur between identical fluorophores, such as two mGFPs, which is called homo-FRET (Bader et al., 2011). As the acceptor fluorophore has the same spectral properties as the donor, homo-FRET can only be detected by the decrease in fluorescence polarization, due to the additional depolarization by the acceptor. Given that only one fluorophore is employed, homo-FRET cannot be used to detect the interaction between two different proteins, as homo- and heterotypic interactions could not be distinguished. Hence its application has been somewhat limited.

However, homo-FRET is highly interesting to study the transport, nanoclustering, an organization of membrane proteins, such as has initially been shown for GPI-anchored proteins (Varma and Mayor, 1998). The fact that only one fluorescently tagged construct has to be expressed in cells has also advantages for potential applications in compound screening for drugs that interfere with transport or nanoclustering, e.g. when generating a stable cell line. Yet, applications of homo-FRET in cell-based chemo-genetic screens have been rather limited in drug discovery (Yi et al., 2015). By contrast, fluorescence anisotropy/ polarization read-outs are very well established for in vitro high-throughput screening applications (Uri and Nonga, 2020).

Here we developed fluorescence polarization/ anisotropy assays foremost carried out on a fluorescence plate reader to detect the Ras-nanoclustering dependent increase in homo-FRET. We show that the loss of the FRET signal is suitable to detect chemical or genetic modulators of Ras-nanoclustering and any molecular perturbation upstream of it (i.e. lipid modification and trafficking of Ras). By utilizing the Ras-dimerizer BI-2852, we can also detect competitive binding of switch II-pocket binders, such as AMG 510.

2. Materials and methods

2.1. Materials

Mevastatin (J61357, Alfa Aeser), Cycloheximide (0970, Fisher Scientific), Actinomycin D (11421, Cayman), Anisomycin (11308, Cayman), FTI-277 HCl salt (2874, BioVision), GGTI-298 TFA salt (S7466, Slleckchem), Deltarasin (S7224, Selleckchem), Calmidazolium chloride (sc-201494, Santa Cruz), AMG 510 (HY-114277, MedChemExpress) and BI-2852 (S8959, Selleckchem) were commercially acquired from the sources given in parenthesis. siRNA for *CALM1* (Hs_CALM1_6, SI02224222), *FNTA* (Hs_FNTA_6, SI02661995), and the negative RNA control (1027310) were from Qiagen. siRNA for *PDE6D* was from Dharmacon (L-004310–00–0005). pmGFP-CTH, pmGFP-CTK, pmGFP-K-RasG12V and pmGFP-H-RasG12V plasmids were previously described by us (Najumudeen et al., 2015a). pDest305-CMV-mGFP-K-RasG12C plasmid was produced by multi-site gateway cloning using the entry clones acquired from NCI Ras Initiative, USA and Addgene (RAS mutant clone collection, Kit #1000000089).

2.2. Cell Culture, transfections, and homo-FRET measurement

BHK-21 and HEK293-EBNA cells were cultured in Dulbecco's modified Eagle's medium (DMEM) (cat. no. 41965–039, Gibco, Thermo Fisher Scientific) supplemented with 10% v/v fetal bovine serum (FBS) (cat. no. 10270–098, Gibco, Thermo Fisher Scientific), 2 mM L-glutamine (cat. no. 25030–024, Gibco, Thermo Fisher Scientific), and 1% v/v penicillin-streptomycin (cat. no. 15140122, Gibco, Thermo Fisher Scientific). For homo-FRET assays, cells were cultured in 6- or 12-well plates and transfected respectively with 1 and 2 μg of pmGFP-CTH or pmGFP-CTK or pmGFP plasmids using jetPRIME (cat. no. 114–75, Polyplus) according to the manufacturer's instructions. On the next day cells were transferred to a black 96-well plate (cat. no. 655090, Greiner Bio-One) with a density of 5×10^4 for BHK-21 cells and 2×10^5 for HEK293-EBNA cells per well. Inhibitors were added to cells 24 h after transfection and incubated for an additional 24 h. In case of BHK-21 cells, the cell culture medium was replaced with Ringer's buffer (10 mM HEPES, 10 mM glucose, 2 mM NaH_2PO_4, 1 mM $MgCl_2$, 2 mM $CaCl_2$, 5 mM KCl, 155 mM NaCl, pH 7.2) before measurements and the anisotropy readings were taken at 37 °C. HEK293-EBNA cells were directly plated in phenol-red free DMEM (cat. no. 21063029, Gibco, Thermo Fisher Scientific) containing 10% v/v FBS and measurements were taken in this medium at room temperature.

2.3. Fluorescence anisotropy imaging

All fluorescence images were obtained on a Zeiss LSM 780 fluorescence microscope (Carl Zeiss AG, Jena, Germany) using a 10x objective (NA 0.3). Excitation was done using the inbuilt 488 nm Argon laser with an output power of 35 mW. Detection was done using the inbuilt photomultiplier detector of the Zeiss microscope and with wavelengths selected between 493 and 598 nm. Two polarizers fitted in a filter slider placed in front of the camera and aligned parallel and perpendicular to a polarizer placed in the excitation path were used to obtain the parallel and perpendicular images. Images were collected sequentially using the two differently aligned polarizers. Exposure time was ~ 20 s and the two sequential images were collected within 25 s of each other. Images were taken using a pinhole of 1 AU and in a 1024 × 1024 format.

The anisotropy value, r was calculated for each pixel using the Zen software that controls the microscope using the formula mentioned in "Homo-FRET measurements" section. For this particular system, a correction factor G (λ) was calculated using a solution of 10 mM fluorescein in 0.1 M Tris, pH 9.0 in an isotropic medium and found to be 0.94. ImageJ software (National Institutes of Health, USA) with a custom designed look-up-table (LUT) was used to visualize the anisotropy values (r) in rainbow colors in the cells ($0 < r < 0.375$). Anisotropy values of pixels where there are no cells are displayed in white ($r = 0$) or in black ($r > 0.375$). Histograms of the different anisotropy values on each pixel were obtained using ImageJ and then median values were calculated. Pixels without cells were excluded from this calculation.

2.4. Homo-FRET measurements

The depolarization changes originating from the homo-FRET were quantitated by steady-state fluorescence anisotropy measurements (Bader et al., 2011; Chan et al., 2011) with either a BioTek Synergy H1 hybrid fluorescence plate reader (Agilent) or a Clariostar plate reader (BMG Labtech) equipped with a polarization filter cube. Using the Synergy H1 plate reader, fluorescence anisotropy measurements were performed using a BP 485/20 excitation filter and BP 528/20 nm emission filter. Parallel and perpendicular emissions were acquired sequentially. A gain value of 60 was applied for both parallel and perpendicular channels. In the case of the Clariostar plate reader, fluorescence anisotropy measurements were performed using a 482/16 nm excitation filter and 530/40 nm emission filter. Both parallel and perpendicular emissions were acquired simultaneously. An automatic gain setting adjustment was applied for each measurement. For CTH and CTK constructs the gain values were ~800 – 850 and for full-length Ras constructs the gain values were ~ 1000 – 1100 for parallel and perpendicular polarizers.

Fluorescence anisotropies were calculated from the measured fluorescence intensities, according to,

$$r = \frac{I_v - G(\lambda) I_h}{I_v + 2G(\lambda) I_h}$$

where r is the fluorescence anisotropy, I_v is the fluorescence emission intensity detected with vertical polarization, I_h is the fluorescence emission intensity detected with horizontal polarization. The correction factor $G(\lambda) = 1$ for most of the plate readers for λ between 300 and 700 nm, the value 1 was applied for anisotropy measurements in both instruments.

2.5. siRNA knockdown and homo-FRET measurement

On day 1, about 2×10^5 HEK293-EBNA cells were seeded per well of a 12-well plate in complete DMEM. On day 2, cells were transfected with 100 nM of siRNA using 3.5 μl of Lipofectamine RNAiMAX (cat. no. 13778, Thermo Fisher Scientific) reagent and Opti-MEM (cat. no. 31985062, Gibco, Thermo Fisher Scientific) as vehicle. On day 3 the medium was replaced with fresh medium and 1 μg of pmGFP-CTK or pmGFP-CTH plasmid was transfected using 3 μl of jetPRIME reagent. On Day 4 the cells were collected by trypsination and seeded in a 96-well plate and incubated for 18 – 24 h at 37 °C in a cell culture incubator. On day 5 the fluorescence anisotropy readings were taken on the Clariostar plate reader.

2.6. Preparation of PEI reagent and transfection

Linear polyethylenimine (PEI) MW 25000 of transfection grade was from Polysciences Inc. (cat. no. 23966). A 1 mg/ ml solution of PEI was prepared in HPLC grade water. The PEI solution was magnetically stirred and dissolved by adjusting the pH to 6.5–7.5 using HCl at room temperature. After about 4 – 6 h of continuous stirring and constant addition of HCl, a clear PEI solution was obtained with a final pH of 6.8. The PEI solution was sterile filtered using a 0.22 μm Steriflip (Millipore) vacuum filter system. The obtained solution was stored at – 20 °C.

Before every transfection the PEI solution was warmed to 37 °C in a water bath. 60 μl of PEI solution was mixed with 1 ml of serum free DMEM. For transfection of 1–5 μg of plasmid per 10 cm^2 petri dish, the plasmid was diluted in 800 μl of serum free DMEM and 848 μl of PEI/ DMEM mix was added. This complex was incubated for 15 min and then added to cells without further medium exchange.

2.7. Dose-response analysis of inhibitors

On day 1 about 2.5 x 10^6 HEK293-EBNA cells were seeded per 10 cm^2 petri dish in 10 ml DMEM supplemented with 10% v/v FBS. On day 2 cells were transfected with 3 μg of plasmid using the home-made PEI reagent. After 48 h expression on day 4, the cells were collected by trypsination and counted. Then 2×10^5 cells were plated per well of a black 96-well plate in 50 μl phenol-red free complete DMEM. Cells were allowed to settle for 4 h. Then a 2-fold dilution series of inhibitors starting from 40 or 80 μM was prepared in 50 μl phenol-red free complete DMEM and added to cells. The plate was then incubated for 18 h at 37 °C in a cell culture incubator. On day 5, fluorescence anisotropy measurements were taken on the Clariostar plate reader.

2.8. Data and statistical analysis

The number of biological replicates, n, for each experiment is given in the figure legends. The fluorescence anisotropy values after each

measurement were directly obtained from Gen5 or MARS software for Synergy H1 and Clariostar plate readers, respectively. Data analysis was performed in Excel (Microsoft Office 365) and the graphs were prepared using Prism 9 (GraphPad) software.

The Z′ score was determined using the formula,

$$Z' = 1 - \frac{3(\sigma_p + \sigma_n)}{|\mu_p - \mu_n|},$$

where σ_p and σ_n are standard deviations of positive and negative controls respectively, while μ_p and μ_n are the mean values of positive and negative control respectively.

For dose-response curves, the log concentration of inhibitor vs anisotropy value data was plotted and fit into log (agonist) vs response equation (three parameters) equation in Prism and the EC50 values were calculated. Statistical significance was analyzed in Prism using tests as indicated in the figure legends. Comparisons are as indicated or relative to the control sample. A p-value < 0.05 is considered statistically significant, and the statistical significance levels are annotated as follows: * $p < 0.05$; * * $p < 0.01$; * ** $p < 0.001$; * ** * $p < 0.0001$, or ns = not significant.

3. Results and discussion

A H-Ras-derived nanoclustering-FRET biosensor allows to detect drug-induced loss of membrane anchorage by global fluorescence anisotropy image analysis.

Nanoclustering dependent FRET reports not only on nanoclustering, but on any upstream process that affects nanoclustering, including correct plasma membrane trafficking and lipid modifications of the protein of interest (Parkkola et al., 2021). We previously demonstrated that nanoclustering-FRET is a reliable readout in chemical or genetic assays screening for modulators of membrane anchored proteins, such as heterotrimeric G proteins, Src-family kinases, and of course Ras family proteins (Abankwa and Vogel, 2007; Coxon et al., 2014; Crouthamel et al., 2010; Kohnke et al., 2012; Najumudeen et al., 2015a; Najumudeen et al., 2016; Najumudeen et al., 2013; Najumudeen et al., 2015b). Homo-FRET measurements allow to detect FRET between identical fluorophores. This simplifies the requirements for nanoclustering-FRET to only one biosensor construct.

We first established fluorescence anisotropy-based homo-FRET measurements of BHK-21 cells transfected with a H-Ras-derived membrane anchor construct, mGFP-CTH, on a confocal microscope. We genetically fused the extended membrane anchor of H-Ras (residues 163–189 of H-Ras, CTH) to the C-terminus of monomeric EGFP (mGFP) and transiently expressed this construct in BHK-21 cells (Fig. 1A). This construct was well transfected and highly expressed in these cells. Subsequently, cells were sequentially imaged in the two polarization channels and anisotropy values were calculated on a pixel-by-pixel basis (Fig. 1B).

To test, whether anisotropy values can report on changes in functional membrane anchorage of the construct, we treated cells with

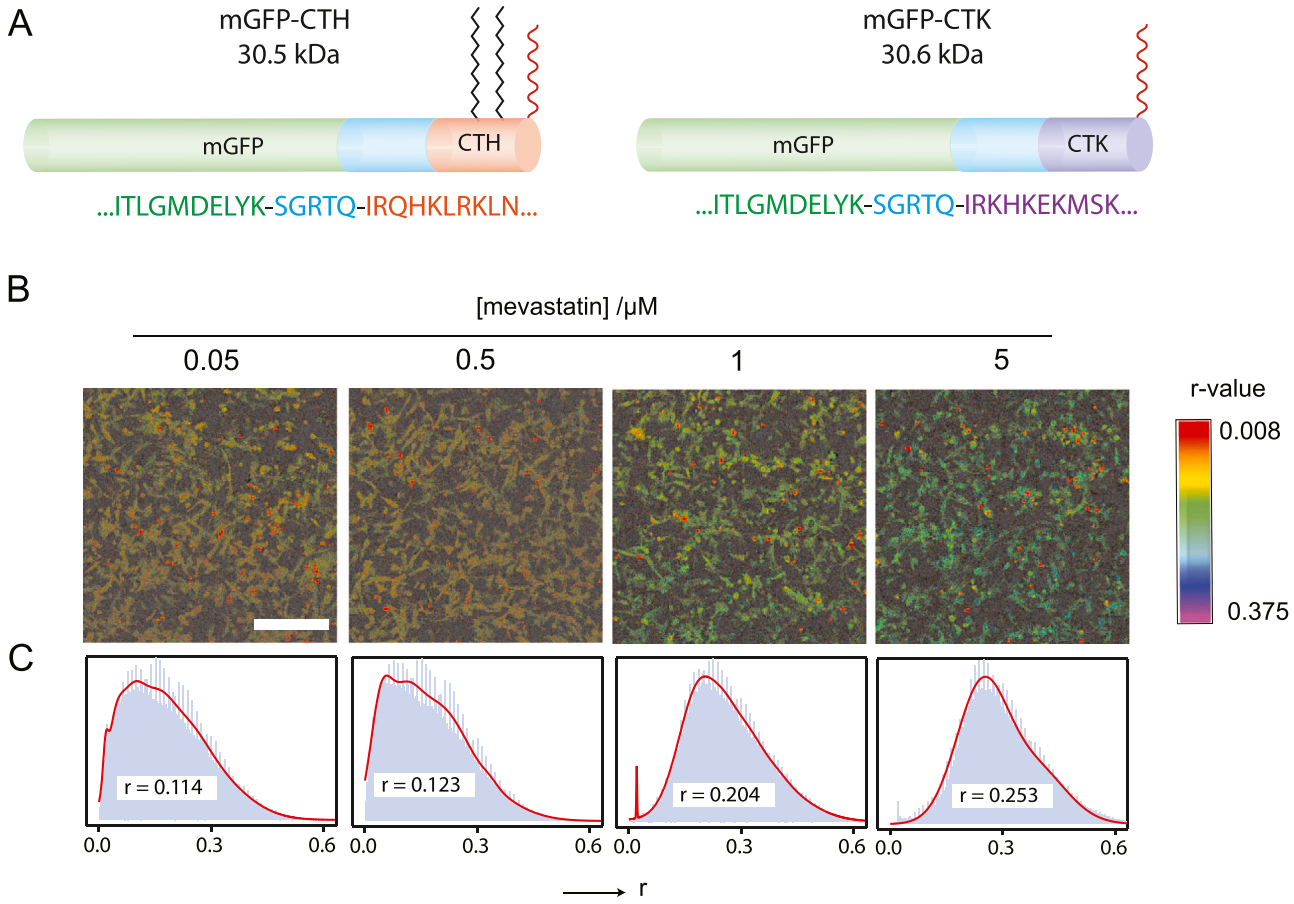

Fig. 1. Confocal microscopy-based anisotropy imaging globally reports on Ras membrane anchorage. (A) Schematic representation of the mGFP-CTH and mGFP-CTK homo-FRET biosensors and their molecular weights are shown. The black zigzag line indicates the palmitoylation at Cys181 and Cys184 in the native H-Ras sequence, while the red zigzag line indicates the farnesylation at Cys186 and Cys185 in the parental sequences of H-Ras and K-Ras, respectively. (B) The mGFP-CTH sensor was transiently expressed in BHK-21 cells, which were treated with indicated concentrations of mevastatin for 24 h. (B) Anisotropy images from a single field of cells are shown as pseudo-colored 8-bit images. Scale bar corresponds to 250 μm. The color lookup table from in the anisotropy images is shown to the right. (C) Global analysis of the anisotropy value distributions. The median values of anisotropy (r) are displayed.

increasing concentrations of mevastatin. Mevastatin is a statin, which inhibits HMG-CoA, the rate-limiting enzyme in the mevalonate pathway that provides the farnesylpyrophosphate-substrate required for Ras farnesylation (Nguyen et al., 2011). Across the images, anisotropy values varied broadly (Fig. 1**B**). However, analysis of the distribution of these values in histograms revealed that the median values increased with increasing concentrations of mevastatin (Fig. 1C). This increased anisotropy value is consistent with a loss of homo-FRET, which leads to an increase in fluorescence anisotropy.

The drug-induced loss of membrane anchorage of the mGFP-CTH construct disrupts the dense packing of the mGFP-CTH proteins in nanoclusters. More generally, the change in dimensionality from the 2D membrane to the 3D cytoplasm lowers the effective concentration and thus the average distance between the FRET-constructs. Similar observations were made previously using hetero-FRET experiments, where also a decrease of initially high FRET levels in cells was found after drug treatment (Kohnke et al., 2012; Parkkola et al., 2021).

While confocal imaging-based fluorescence anisotropy measurements could provide a pixel-level resolution of anisotropy changes, this particular application may be less interesting, as only identical constructs can be studied. Imaging based FRET-experiments more commonly study interactions of two different proteins, such as we demonstrated for Ras and the Ras binding domains of its effectors (Abankwa et al., 2010; Guzman et al., 2014b).

3.1. Plate reader-based homo-FRET measurements can detect the effect of positive and negative modulators of Ras-construct membrane organization

Given that the drug-induced change in fluorescence anisotropy was readily detectable by the global image analysis (Fig. 1 C), we next established homo-FRET measurements on a multi-mode fluorescence plate reader that was equipped with polarization filter-cubes. Similar to the global image analysis, the signal is here collected across a number of cells in the sample.

BHK-21 cells were transfected with mGFP or mGFP-CTH and then split into 96-well plates for fluorescence anisotropy readings in a plate reader. Before the measurement, the culture medium was replaced with Ringer's buffer. The mGFP-CTH produced a significantly lower anisotropy value compared to mGFP alone, due to the nanoclustering-specific homo-FRET signal (Fig. 2A). When mGFP-CTH expressing cells were treated with mevastatin, we observed a dose-dependent increase in the fluorescence anisotropy, consistent with a loss of homo-FRET after inhibition of membrane anchorage of the mGFP-CTH construct (Fig. 2B). Note that the absolute anisotropy values determined on the plate reader differed from those measured by imaging (Fig. 1), given that the instrument-specific correction factor G(λ) was not determined.

After mevastatin treatment the anisotropy value is expected to approach that of the free mGFP (Fig. 2A,B). However, the mGFP value is somewhat lower, which we explain by the very high expression level of this construct, as compared to the membrane anchored constructs. This may increase the probability of homo-FRET in the cytoplasm, eventually even due to some aggregation.

3.2. Optimized assay conditions allow to quantitate the effect of Ras-lipidation and -trafficking inhibitors

For the following experiments, we changed our experimental platform, employing a different plate reader (Clariostar, BMG Labtech) and expressing constructs in HEK293-EBNA (HEK) cells, which are optimized for high protein expression. In addition to the mGFP-CTH biosensor, we now also tested an analogous construct, mGFP-CTK, which employed the C-terminal membrane anchor of K-Ras (residues 163–188, CTK) (Fig. 1 A).

The fluorescence anisotropy signals of HEK cells expressing either mGFP, mGFP-CTH or mGFP-CTK were directly obtained from cells grown in phenol-red free medium. Under these improved conditions, a significantly increased dynamic range becomes apparent (Fig. 3A). Both constructs, mGFP-CTH and mGFP-CTK showed a significantly lower anisotropy value than mGFP alone, consistent with a nanoclustering-specific increase in homo-FRET. Note that absolute values on this platform differed from the previous ones (Figs. 1 and 2), as again no correction factor G(λ) was applied.

Next, we tested whether an increase in homo-FRET can also be detected. We previously showed that natural products, such as protein synthesis inhibitor anisomycin and chemotherapeutic actinomycin D, a transcription inhibitor, can increase the FRET of mGFP-CTH (Najumudeen et al., 2015a). Consistent with our previous observations, treatment with anisomycin (Fig. 3B) or actinomycin D (Fig. 3 C), led to a notable decrease in anisotropy, respectively an increase in homo-FRET.

In order to establish that these biosensors can be exploited for chemo-genetic screening, we determined the Z′-factors, which are typically used to assess the goodness of an assay for high-throughput screening (Zhang et al., 1999) (Fig. 3D,E). The Z′-factor ranges from 0 to 1, and a Z′ of > 0.5 is considered excellent, while smaller ones are

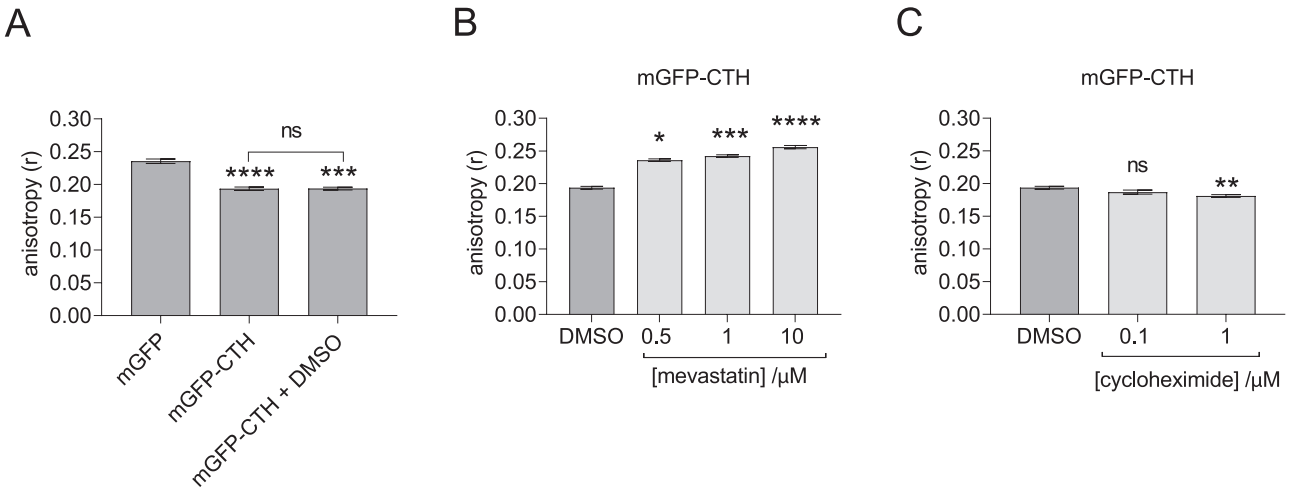

Fig. 2. Establishment of a plate reader-based homo-FRET assay in BHK-21 cells. (A) Comparison of anisotropy values from BHK-21 cells expressing mGFP and mGFP-CTH. (B,C) Effect of mevastatin (B) and cycloheximide (C) on the fluorescence anisotropy of BHK-21 cells expressing mGFP-CTH. Cells were treated with indicated concentrations of inhibitors or 0.2% v/v DMSO in medium (DMSO) for 24 h before the anisotropy measurement. Anisotropy readings were taken in Ringer's solution using a BioTek Synergy H1 (Agilent) plate reader. All data in this figure represent mean ± SEM of n = 12 replicates per condition and statistical analysis was performed using Kruskal-Wallis test.

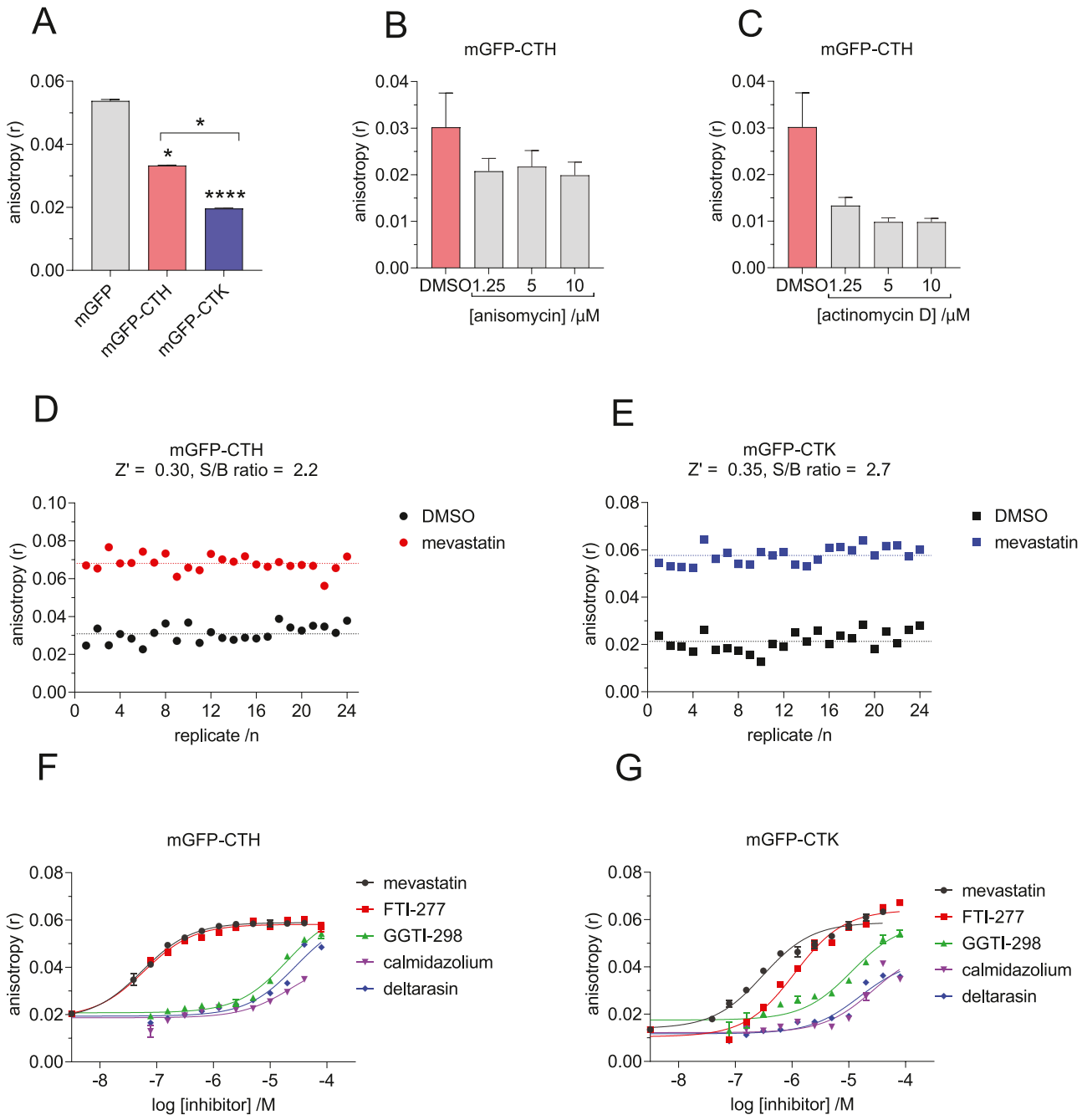

Fig. 3. Establishment of an optimized plate reader-based homo-FRET assay in HEK293-EBNA cells. (A) Comparison of the anisotropy values from HEK293-EBNA cells after 48 h expression of mGFP-CTH, mGFP-CTK or mGFP alone. Data represent mean ± SEM of n = 8 replicates and statistical analysis was performed using Kruskal-Wallis test. (B, C) Effect of anisomycin (B) and actinomycin D (C) on the fluorescence anisotropy of HEK-293EBNA cells expressing mGFP-CTH. The biosensor was expressed for 48 h followed by 24 h treatment with indicated concentrations of compounds or DMSO control (0.8% v/v in medium). Data represent mean ± SEM of n = 2–4 replicates. (D, E) Z′ values and signal-to-background (S/B) ratio from HEK293-EBNA cells expressing either mGFP-CTH (D) or mGFP-CTK (E) treated for 24 h with 10 μM mevastatin or DMSO control (0.2% v/v in medium). For mGFP-CTH (D), the mean ± SD values for positive control (mevastatin) and negative control (DMSO) were 0.068 ± 0.004 and 0.031 ± 0.004, respectively. For mGFP-CTK (E), the mean ± SD values for positive control (mevastatin) and negative control (DMSO) were 0.058 ± 0.004 and 0.021 ± 0.004, respectively. The number of samples was n = 24 for both biosensors. (F, G) Dose response analysis of various Ras membrane anchorage inhibitors using mGFP-CTH (F) and mGFP-CTK (G) biosensors expressed for 48 h followed by inhibitor treatment for 18 h. Data represent mean ± SEM of n = 3 replicates. All readings in this and subsequent figures were taken in phenol red-free DMEM with 10% v/v FBS using a Clariostar (BMG Labtech) plate reader.

also acceptable, as long as the value stays positive. Mevastatin was used as the positive control, which increased the homo-FRET signal of both mGFP-CTH and mGFP-CTK expressing cells. In order to improve the assay also economically, we here used the inexpensive home-made polyethylenimine (PEI) reagent for transfections. An acceptable Z′ of ≥ 0.3 and a signal-to-background ratio of > 2 were determined, indicating the suitability of the assay for screening (Fig. 3D,E). Previously, we observed Z′ values of more than 0.8 using lipofection, suggesting that the lower value observed here is the result of less-efficient transfection using the PEI reagent. Further assay optimizations, such of transfection conditions or redesign of the biosensors, may improve the screening assay parameters.

In order to further validate the suitability of this assay for compound screening, we transfected cells using PEI and analyzed the effect of five inhibitors of Ras-lipidation or -trafficking on the homo-FRET of mGFP-CTH (Fig. 3F) and mGFP-CTK (Fig. 3G). In addition to mevastatin, we tested the farnesyl-transferase (FTase) inhibitor FTI-277 and the geranylgeranyl-transferase I (GGTase I) inhibitor GGTI-298, which block attachment of the respective lipid moieties to Ras.

In line with the farnesylation of both parental Ras proteins, H-Ras and K-Ras, the anisotropy of both biosensors increased with higher concentrations of FTI-277 showing an EC50-value that was as low as that of mevastatin in the case of mGFP-CTH (Table 1). However, for mGFP-CTK the EC50-value was higher, consistent with the possibility that K-Ras can undergo alternative prenylation by GGTase I (Fiordalisi et al., 2003). Conversely, the EC50 of mGFP-CTK for GGTI-298 treatment was lower than that of mGFP-CTH (Table 1).

In addition, we tested inhibitors of two trafficking chaperones of Ras, which both have a preference for K-Ras in cells (Okutachi et al., 2021; Siddiqui et al., 2020). We tested the effect of the calmodulin inhibitor calmidazolium and of the PDE6D inhibitor deltarasin on the homo-FRET of both biosensors (Prozialeck and Weiss, 1982; Zimmermann et al., 2013). Within the tested concentration regime, we could not reach full inhibition, hence the EC50 values are only approximations. In line with previous observations, calmidazolium affected both the H-Ras and K-Ras derived biosensors, while deltarasin showed a slight mGFP-CTK selectivity (Table 1) (Okutachi et al., 2021; Siddiqui et al., 2020).

As long as on plate-controls and the same assay platform is chosen, these screening data are independent from the determination of the absolute anisotropy value. Moreover, different transfection reagents and cell treatment conditions, such as in Fig. 3A as compared to Fig. 3F,G could lead to slight differences in the anisotropy readings even on the same platform.

3.3. Homo-FRET Ras-derived biosensors are also applicable for genetic screening

In addition to chemical screening, genetic screening may be of high interest to identify novel modulators of Ras trafficking and membrane organization. In order to test this, we treated HEK cells with siRNAs against the shared α-subunit of FTase and GGTase I (*FNTA*), calmodulin (*CALM1*) and PDE6D (*PDE6D*) followed by biosensor expression.

The knockdown of *FNTA* led to an increase in anisotropy by ~76% and ~113% for mGFP-CTH and mGFP-CTK, respectively (Fig. 4A,B), which was again consistent with a loss of membrane anchorage of the biosensor constructs as observed with chemical inhibitors against these target proteins (Fig. 3).

The effect of the knockdowns of *CALM1* or *PDE6D* was significantly lower, suggesting that they are not the sole trafficking chaperones that facilitate plasma membrane trafficking of the biosensors, and therefore also the parental Ras isoforms. Consistent with the preference of calmodulin for K-Ras, knockdown of *CALM1* selectively affected the K-Ras derived biosensor mGFP-CTK more than the H-Ras derived biosensor mGFP-CTH (Fig. 4A,B). However, contrary to previous observations, the *PDE6D* knockdown affected mGFP-CTH more than mGFP-CTK. This may be attributed to distinct behaviour of the membrane-anchor only constructs as compared to full-length parental Ras proteins.

Table 1
EC50 values from dose-response curves in Fig. 3F,G. * marks only approximated values.

inhibitor	EC50 /μM (n = 3, mean ± SEM)	
	mGFP-CTH	mGFP-CTK
mevastatin	0.06 ± 0.01	0.31 ± 0.04
FTI-277	0.06 ± 0.02	1.1 ± 0.2
GGTI-298	20 ± 4	12 ± 4
calmidazolium	24 ± 2 *	27 ± 2 *
deltarasin	29 ± 6 *	14.5 ± 0.5 *

3.4. Homo-FRET measurements with full-length Ras confirm response to inhibitors

Finally, we wanted to see, if the homo-FRET of full-length Ras constructs is also sensitive to the treatment with inhibitors of Ras. We constructed N-terminally mGFP-tagged H-RasG12V and K-RasG12V and expressed these biosensors in HEK cells (Fig. 5A,B).

Membrane anchorage via the lipid modifications is likely allowing for restricted, but not rigidified motion of the G-domain in conjunction with the mGFP-fusion. It is therefore plausible to assume that the molecular weight of the whole construct will contribute to the characteristic anisotropy. In agreement with the higher molecular weight of the mGFP- full-length Ras-fusion, which leads to slower rotation or precession, the anisotropy value of the donor-only samples was higher in both cases than that of the membrane anchor-based biosensors (compare Fig. 3A and Fig. 5A,B). Moreover, as for mGFP-CTK, the anisotropy value of mGFP-K-RasG12V was lower than their H-Ras counterparts, indicating a higher homo-FRET and therefore denser packing of oncogenic K-Ras in nanoclusters than H-Ras. This finding is compatible with the higher number of K-Ras proteins per nanocluster as compared to H-Ras proteins that was established by electron microscopy-based investigations (Plowman et al., 2005).

As observed for the membrane anchor constructs (Fig. 3 F,G), treatment with FTI-277 increased the anisotropy as much as mevastatin treatment for mGFP-H-RasG12V, while this was not seen for mGFP-K-RasG12V (Fig. 5 A,B). Conversely, the effect of the GGTI-298 was stronger on mGFP-K-RasG12V than on mGFP-H-RasG12V, confirming the known sensitivities of these Ras proteins to the inhibition of the respective prenyltransferases.

Again the response to the inhibitors of the trafficking chaperones calmodulin, calmidazolium, and PDE6D, deltarasin, was less than that to the lipid-modification inhibitors (Fig. 5A,B). This time, inhibitors more selectively affected the K-RasG12V than the H-RasG12V biosensor, consistent with the preference of the targeted chaperones for K-RasG12V (Chandra et al., 2011; Villalonga et al., 2001). This clear K-Ras selectivity observed with the full-length, but not that well with the membrane anchor constructs, may be due to the contribution from the G-domain of Ras proteins, which may sterically affect the binding to the trafficking chaperones.

Finally, we investigated whether the small molecule BI-2852 that was found to induce non-productive dimers of K-Ras can increase homo-FRET (Tran et al., 2020). This drug was originally developed as a SOS-inhibitor that binds to the switch I/II pocket of Ras (Kessler et al., 2019). Recently, the Shokat group utilized a fluorescent derivative in an innovative assay that can detect switch II pocket binders of K-Ras, such as covalent K-RasG12C inhibitor AMG 510 (Vasta et al., 2022).

We therefore compared the fluorescence anisotropy of cells expressing mGFP-K-RasG12C treated either with increasing concentrations of BI-2852 alone, or after 4 h pretreatment with 5 μM AMG 510, which was expected to block the binding site of BI-2852. In agreement with this, BI-2852 decreased the anisotropy significantly already at 5 μM (Fig. 5C). This was significantly blocked by pre-treatment with AMG 510, confirming the switch II pocket dependence of the forced dimerization by BI-2852.

4. Conclusions

We conclude that for testing of and eventually screening for chemical compounds or genetic-dependencies that modulate Ras trafficking or of switch II pocket binders the investigated homo-FRET biosensors are well suitable. Fluorescence anisotropy measurements are less sensitive to the fluorescence intensity variations of the sample and in this context the expression level of the biosensor construct. Therefore, this method is

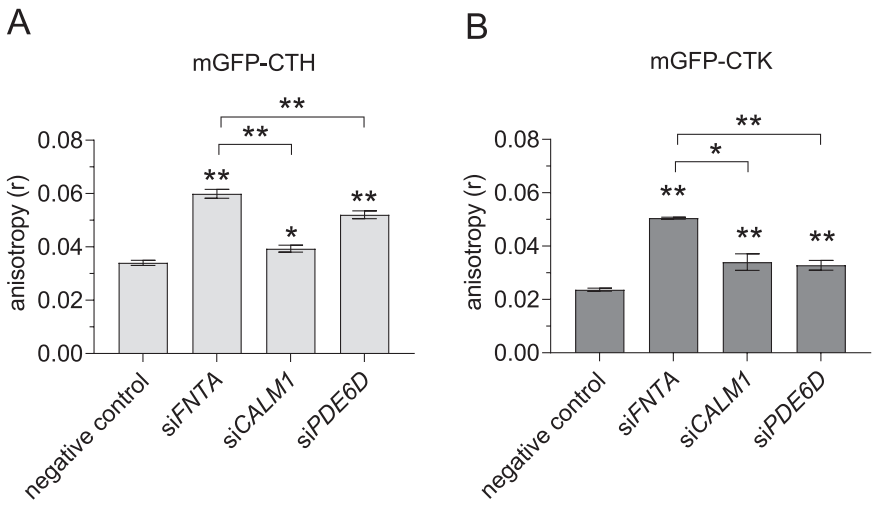

Fig. 4. Effect of siRNA-mediated knockdowns on the fluorescence anisotropy of mGFP-CTH and mGFP-CTK biosensors. (A,B) HEK293-EBNA cells were transfected with siRNA for 24 h followed by pmGFP-CTH (A) or pmGFP-CTK (B) construct transfection. After 48 h of expression, fluorescence anisotropy measurements were performed. Data represent average ± SEM of n = 4–6 replicates. Statistical analysis was performed using Mann Whitney test.

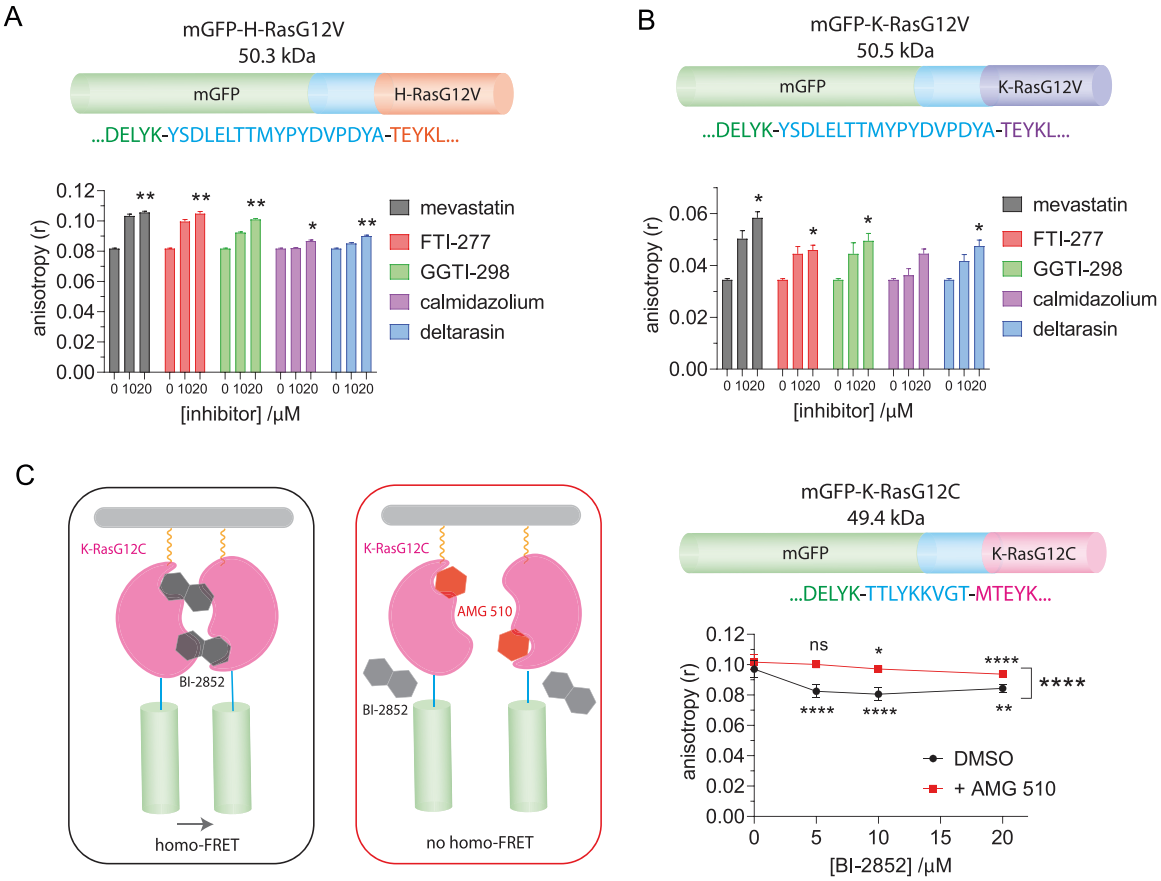

Fig. 5. Effect of Ras membrane anchorage inhibitors and Ras-dimerizing BI-2852 on the fluorescence anisotropy of mGFP-tagged full-length Ras biosensors. (A,B) HEK293-EBNA cells were transfected with plasmids encoding mGFP-H-RasG12V (A) or mGFP-K-RasG12V (B), which were expressed for 48 h. The schematic representations of each biosensor and their molecular weights are shown. Cells expressing mGFP-H-RasG12V or mGFP-K-RasG12V were treated with inhibitors at indicated concentrations for 18 h followed by the fluorescence anisotropy measurements. Data represent mean ± SEM of n = 4 replicates and statistical analysis was performed using Kruskal-Wallis test. (C) Schematic representation of the homo-FRET assay employing mGFP-K-RasG12C and BI-2852. The mGFP-K-RasG12C expressing HEK-293EBNA cells were treated with 5 μM AMG 510 for 4 h followed by BI-2852 treatment for another 4 h before the anisotropy measurement (+ AMG 510); DMSO control is 0.05% v/v in medium, without pretreatment with AMG 510 (DMSO). Data represent mean ± SEM of n = 12 replicates and statistical analysis was performed using Kruskal-Wallis and Mann Whitney tests.

suitable to compare constructs with somewhat different expression levels, such as mGFP-H-RasG12V with a higher expression as compared to mGFP-K-RasG12V. Moreover, anisotropy values can qualitatively be related to the extent of clustering of Ras protein constructs, thus providing also basic biological information.

Given the advantage that only one biosensor construct has to be expressed, we propose to employ anisotropy measurements for the detection of homo-FRET more broadly in applications that detect the functional membrane organization of peripheral membrane proteins, such as Ras-, Rho-, Rab-, Arf-, Src-family and heterotrimeric G-proteins.

CRediT authorship contribution statement

Ganesh babu Manoharan: Conceptualisation, Methodology, Investigation, Data curation, Writing – original draft, Formal Analysis, Visualisation. **Camilo Guzman:** Conceptualisation, Methodology, Investigation, Formal Analysis. **Arafath Kaja Najumudeen:** Methodology, Investigation, Formal analysis. **Daniel Abankwa:** Conceptualisation, Writing – original draft, Writing – review & editing, Supervision, Funding acquisition.

Declaration of Competing Interest

The authors declare that they have no known competing financial interests or personal relationships that could have appeared to influence the work reported in this paper.

Data Availability

Data will be made available on request.

Acknowledgements

The study was supported by internal funds of the University of Luxembourg, Luxembourg, the Academy of Finland and the Sigrid Juselius Foundation, Finland. We are thankful to Dominic Esposito and Vanessa Wall (Frederick National Laboratory for Cancer Research, Frederick, MD, United States) for providing the entry clones and destination vectors for multisite gateway cloning. We thank Mrs. Nesrine Ben Fredj and Mrs. Christina Laurini for the technical assistance.

References

Abankwa, D., Gorfe, A.A., 2020. Mechanisms of ras membrane organization and signaling: ras rocks again. Biomolecules 10.

Abankwa, D., Vogel, H., 2007. A FRET map of membrane anchors suggests distinct microdomains of heterotrimeric G proteins. J. Cell Sci. 120, 2953–2962.

Abankwa, D., Hanzal-Bayer, M., Ariotti, N., Plowman, S.J., Gorfe, A.A., Parton, R.G., McCammon, J.A., Hancock, J.F., 2008. A novel switch region regulates H-ras membrane orientation and signal output. EMBO J. 27, 727–735.

Abankwa, D., Gorfe, A.A., Inder, K., Hancock, J.F., 2010. Ras membrane orientation and nanodomain localization generate isoform diversity. Proceedings of the National Academy of Sciences 107, 1130–1135.

Bader, A.N., Hoetzl, S., Hofman, E.G., Voortman, J., van Bergen en Henegouwen, P.M., van Meer, G., Gerritsen, H.C., 2011. Homo-FRET imaging as a tool to quantify protein and lipid clustering. ChemPhysChem 12, 475–483.

Blazevits, O., Mideksa, Y.G., Solman, M., Ligabue, A., Ariotti, N., Nakhaeizadeh, H., Fansa, E.K., Papageorgiou, A.C., Wittinghofer, A., Ahmadian, M.R., Abankwa, D., 2016. Galectin-1 dimers can scaffold Raf-effectors to increase H-ras nanoclustering. Sci. Rep. 6, 24165.

Castel, P., Rauen, K.A., McCormick, F., 2020. The duality of human oncoproteins: drivers of cancer and congenital disorders. Nat. Rev. Cancer 379, 1–15.

Chan, F.T., Kaminski, C.F., Kaminski Schierle, G.S., 2011. HomoFRET fluorescence anisotropy imaging as a tool to study molecular self-assembly in live cells. ChemPhysChem 12, 500–509.

Chandra, A., Grecco, H.E., Pisupati, V., Perera, D., Cassidy, L., Skoulidis, F., Ismail, S.A., Hedberg, C., Hanzal-Bayer, M., Venkitaraman, A.R., Wittinghofer, A., Bastiaens, P.I., 2011. The GDI-like solubilizing factor PDEdelta sustains the spatial organization and signalling of Ras family proteins. Nat. Cell Biol. 14, 148–158.

Cox, A.D., Der, C.J., Philips, M.R., 2015. Targeting RAS membrane association: back to the future for anti-RAS Drug Discovery? Clinical cancer research. Off. J. Am. Assoc. Cancer Res. 21, 1819–1827.

Coxon, F.P., Joachimiak, L., Najumudeen, A.K., Breen, G., Gmach, J., Oetken-Lindholm, C., Way, R., Dunford, J.E., Abankwa, D., Blazewska, K.M., 2014. Synthesis and characterization of novel phosphonocarboxylate inhibitors of RGGT. Eur. J. Med Chem. 84, 77–89.

Crouthamel, M., Abankwa, D., Zhang, L., DiLizio, C., Manning, D.R., Hancock, J.F., Wedegaertner, P.B., 2010. An N-terminal polybasic motif of Galphaq is required for signaling and influences membrane nanodomain distribution. Mol. Pharmacol. 78, 767–777.

Fiordalisi, J.J., Johnson 2nd, R.L., Weinbaum, C.A., Sakabe, K., Chen, Z., Casey, P.J., Cox, A.D., 2003. High affinity for farnesyltransferase and alternative prenylation contribute individually to K-Ras4B resistance to farnesyltransferase inhibitors. J. Biol. Chem. 278, 41718–41727.

Gorfe, A.A., Hanzal-Bayer, M., Abankwa, D., Hancock, J.F., McCammon, J.A., 2007. Structure and dynamics of the full-length lipid-modified H-Ras protein in a 1,2-dimyristoylglycero-3-phosphocholine bilayer. J. Med. Chem. 50, 674–684.

Grant, B.M.M., Enomoto, M., Back, S.I., Lee, K.Y., Gebregiworgis, T., Ishiyama, N., Ikura, M., Marshall, C.B., 2020. Calmodulin disrupts plasma membrane localization of farnesylated KRAS4b by sequestering its lipid moiety. Sci. Signal. 13.

Guzman, C., Solman, M., Abankwa, D., 2014a. Nanoclustering and heterogeneous membrane diffusion of Ras studied by FRAP and RICS analysis. Methods Mol. Biol. 1120, 307–326.

Guzman, C., Solman, M., Ligabue, A., Blazevits, O., Andrade, D.M., Reymond, L., Eggeling, C., Abankwa, D., 2014b. The efficacy of Raf kinase recruitment to the GTPase H-ras depends on H-ras membrane conformer-specific nanoclustering. J. Biol. Chem. 289, 9519–9533.

Guzman, C., Oetken-Lindholm, C., Abankwa, D., 2016. Automated high-throughput fluorescence lifetime imaging microscopy to detect protein-protein interactions. J. Lab Autom. 21, 238–245.

Kattan, W.E., Liu, J., Montufar-Solis, D., Liang, H., Brahmendra Barathi, B., van der Hoeven, R., Zhou, Y., Hancock, J.F., 2021. Components of the phosphatidylserine endoplasmic reticulum to plasma membrane transport mechanism as targets for KRAS inhibition in pancreatic cancer. Proceedings of the National Academy of Sciences 118.

Kessler, D., Gmachl, M., Mantoulidis, A., Martin, L.J., Zoephel, A., Mayer, M., Gollner, A., Covini, D., Fischer, S., Gerstberger, T., Gmaschitz, T., Goodwin, C., Greb, P., Haring, D., Hela, W., Hoffmann, J., Karolyi-Oezguer, J., Knesl, P., Kornigg, S., Koegl, M., Kousek, R., Lamarre, L., Moser, F., Munico-Martinez, S., Peinsipp, C., Phan, J., Rinnenthal, J., Sai, J., Salamon, C., Scherbantin, Y., Schipany, K., Schnitzer, R., Schrenk, A., Sharps, B., Siszler, G., Sun, Q., Waterson, A., Wolkerstorfer, B., Zeeb, M., Pearson, M., Fesik, S.W., McConnell, D.B., 2019. Drugging an undruggable pocket on KRAS. Proceedings of the National Academy of Sciences 116, 15823–15829.

Kohnke, M., Schmitt, S., Ariotti, N., Piggott, A.M., Parton, R.G., Lacey, E., Capon, R.J., Alexandrov, K., Abankwa, D., 2012. Design and application of in vivo FRET biosensors to identify protein prenylation and nanoclustering inhibitors. Chem. Biol. 19, 866–874.

Li, Z., Janosi, L., Gorfe, A.A., 2012. Formation and domain partitioning of H-ras peptide nanoclusters: effects of peptide concentration and lipid composition. J. Am. Chem. Soc. 134, 17278–17285.

Murakoshi, H., Iino, R., Kobayashi, T., Fujiwara, T., Ohshima, C., Yoshimura, A., Kusumi, A., 2004. Single-molecule imaging analysis of Ras activation in living cells. Proceedings of the National Academy of Sciences 101, 7317–7322.

Najumudeen, A.K., Kohnke, M., Solman, M., Alexandrov, K., Abankwa, D., 2013. Cellular FRET-biosensors to detect membrane targeting inhibitors of N-myristoylated proteins. PLoS One 8, e66425.

Najumudeen, A.K., Guzman, C., Posada, I.M., Abankwa, D., 2015a. Rab-NANOPS: FRET biosensors for Rab membrane nanoclustering and prenylation detection in mammalian cells. Methods Mol. Biol. 1298, 29–45.

Najumudeen, A.K., Posada, I.M., Lectez, B., Zhou, Y., Landor, S.K., Fallarero, A., Vuorela, P., Hancock, J., Abankwa, D., 2015b. Phenotypic screening identifies protein synthesis inhibitors as H-ras-nanocluster-increasing tumor growth inducers. Biochemistry 54, 7212–7221.

Najumudeen, A.K., Jaiswal, A., Lectez, B., Oetken-Lindholm, C., Guzman, C., Siljamaki, E., Posada, I.M., Lacey, E., Aittokallio, T., Abankwa, D., 2016. Cancer stem cell drugs target K-ras signaling in a stemness context. Oncogene 35, 5248–5262.

Nan, X., Tamguney, T.M., Collisson, E.A., Lin, L.J., Pitt, C., Galeas, J., Lewis, S., Gray, J. W., McCormick, F., Chu, S., 2015. Ras-GTP dimers activate the Mitogen-Activated Protein Kinase (MAPK) pathway. Proceedings of the National Academy of Sciences 112, 7996–8001.

Nguyen, U.T.T., Goodall, A., Alexandrov, K., Abankwa, D., 2011. Isoprenoid modifications. In: Vidal, C.J. (Ed.), Post-Translational Modifications in Health and Disease. Springer, New York, New York, NY, pp. 1–37.

Okutachi, S., Manoharan, G.B., Kiriazis, A., Laurini, C., Catillon, M., McCormick, F., Yli-Kauhaluoma, J., Abankwa, D., 2021. A covalent calmodulin inhibitor as a tool to study cellular mechanisms of K-ras-driven stemness. Front Cell Dev. Biol. 9, 665673.

Parkkola, H., Siddiqui, F.A., Oetken-Lindholm, C., Abankwa, D., 2021. FLIM-FRET analysis of ras nanoclustering and membrane-anchorage. Methods Mol. Biol. 2262, 233–250.

Pavic, K., Chippalkatti, R., Abankwa, D., 2022. Drug targeting opportunities en route to Ras nanoclusters. Adv. Cancer Res 153, 63–99.

Plowman, S.J., Muncke, C., Parton, R.G., Hancock, J.F., 2005. H-ras, K-ras, and inner plasma membrane raft proteins operate in nanoclusters with differential dependence on the actin cytoskeleton. Proceedings of the National Academy of Sciences 102, 15500–15505.

Posada, I.M., Serulla, M., Zhou, Y., Oetken-Lindholm, C., Abankwa, D., Lectez, B., 2016. ASPP2 is a novel pan-ras nanocluster scaffold. PLoS One 11, e0159677.

Prior, I.A., Muncke, C., Parton, R.G., Hancock, J.F., 2003. Direct visualization of Ras proteins in spatially distinct cell surface microdomains. J. Cell Biol. 160, 165–170.
Prozialeck, W.C., Weiss, B., 1982. Inhibition of calmodulin by phenothiazines and related drugs: structure-activity relationships. J. Pharmacol. Exp. Ther. 222, 509–516.
Punekar, S.R., Velcheti, V., Neel, B.G., Wong, K.K., 2022. The current state of the art and future trends in RAS-targeted cancer therapies. Nat. Rev. Clin. Oncol. 19, 637–655.
Rizzo, M.A., Piston, D.W., 2005. High-contrast imaging of fluorescent protein FRET by fluorescence polarization microscopy. Biophys. J. 88, L14–16.
Rizzo, M.A., Springer, G.H., Granada, B., Piston, D.W., 2004. An improved cyan fluorescent protein variant useful for FRET. Nat. Biotechnol. 22, 445–449.
Sarkar-Banerjee, S., Sayyed-Ahmad, A., Prakash, P., Cho, K.J., Waxham, M.N., Hancock, J.F., Gorfe, A.A., 2017. Spatiotemporal analysis of K-ras plasma membrane interactions reveals multiple high order homo-oligomeric complexes. J. Am. Chem. Soc. 139, 13466–13475.
Schmick, M., Kraemer, A., Bastiaens, P.I., 2015. Ras moves to stay in place. Trends Cell Biol. 25, 190–197.
Siddiqui, F.A., Alam, C., Rosenqvist, P., Ora, M., Sabt, A., Manoharan, G.B., Bindu, L., Okutachi, S., Catillon, M., Taylor, T., Abdelhafez, O.M., Lonnberg, H., Stephen, A.G., Papageorgiou, A.C., Virta, P., Abankwa, D., 2020. PDE6D inhibitors with a new design principle selectively block K-ras activity. ACS Omega 5, 832–842.
Simanshu, D.K., Nissley, D.V., McCormick, F., 2017. RAS proteins and their regulators in human disease. Cell 170, 17–33.
Solman, M., Ligabue, A., Blazevits, O., Jaiswal, A., Zhou, Y., Liang, H., Lectez, B., Kopra, K., Guzman, C., Harma, H., Hancock, J.F., Aittokallio, T., Abankwa, D., 2015. Specific cancer-associated mutations in the switch III region of Ras increase tumorigenicity by nanocluster augmentation. eLife 4, e08905.
Tran, T.H., Alexander, P., Dharmaiah, S., Agamasu, C., Nissley, D.V., McCormick, F., Esposito, D., Simanshu, D.K., Stephen, A.G., Balius, T.E., 2020. The small molecule BI-2852 induces a nonfunctional dimer of KRAS. Proceedings of the National Academy of Sciences 117, 3363–3364.
Uri, A., Nonga, O.E., 2020. What is the current value of fluorescence polarization assays in small molecule screening? Expert Opin. Drug Disco 15, 131–133.
Varma, R., Mayor, S., 1998. GPI-anchored proteins are organized in submicron domains at the cell surface. Nature 394, 798–801.
Vasta, J.D., Peacock, D.M., Zheng, Q., Walker, J.A., Zhang, Z., Zimprich, C.A., Thomas, M.R., Beck, M.T., Binkowski, B.F., Corona, C.R., Robers, M.B., Shokat, K.M., 2022. KRAS is vulnerable to reversible switch-II pocket engagement in cells. Nat. Chem. Biol. 18, 596–604.
Villalonga, P., Lopez-Alcala, C., Bosch, M., Chiloeches, A., Rocamora, N., Gil, J., Marais, R., Marshall, C.J., Bachs, O., Agell, N., 2001. Calmodulin binds to K-Ras, but not to H- or N-Ras, and modulates its downstream signaling. Mol. Cell Biol. 21, 7345–7354.
Yi, N.Y., He, Q., Caligan, T.B., Smith, G.R., Forsberg, L.J., Brenman, J.E., Sexton, J.Z., 2015. Development of a cell-based fluorescence polarization biosensor using preproinsulin to identify compounds that alter insulin granule dynamics. Assay. Drug Dev. Technol. 13, 558–569.
Zhang, J.H., Chung, T.D., Oldenburg, K.R., 1999. A simple statistical parameter for use in evaluation and validation of high throughput screening assays. J. Biomol. Screen 4, 67–73.
Zhou, Y., Prakash, P., Liang, H., Cho, K.J., Gorfe, A.A., Hancock, J.F., 2017. Lipid-sorting specificity encoded in K-ras membrane anchor regulates signal output. Cell 168 (239–251), e216.
Zhou, Y., Gorfe, A.A., Hancock, J.F., 2021. RAS nanoclusters selectively sort distinct lipid headgroups and acyl chains. Front Mol. Biosci. 8, 686338.
Zimmermann, G., Papke, B., Ismail, S., Vartak, N., Chandra, A., Hoffmann, M., Hahn, S. A., Triola, G., Wittinghofer, A., Bastiaens, P.I., Waldmann, H., 2013. Small molecule inhibition of the KRAS-PDEdelta interaction impairs oncogenic KRAS signalling. Nature 497, 638–642.